Molecular Dynamics Simulation of Poly(ethylene terephthalate) Oligomers

Qifei Wang,[†] David J. Keffer,*,[†] Simioan Petrovan,[†] and J. Brock Thomas[‡]

Department of Chemical and Biomolecular Engineering, 1512 Middle Drive, University of Tennessee, Knoxville, Tennessee 37996-2200, and Eastman Chemical Company, Kingsport, Tennessee 37662-5230

Received: October 12, 2009; Revised Manuscript Received: November 23, 2009

Molecular dynamics simulations of poly(ethylene terephthalate) (PET) oligomers are performed in the isobaric−isothermal (NpT) ensemble at a state point typical of a finishing reactor. The oligomer size ranges from 1 to 10 repeat units. We report thermodynamic properties (density, potential energy, enthalpy, heat capacity, isothermal compressibility, and thermal expansivity), transport properties (self-diffusivity, zero-shear-rate viscosity, thermal conductivity), and structural properties (pair correlation functions, hydrogen bonding network, chain radius of gyration, chain end-to-end distance) as a function of oligomer size. We compare the results with existing molecular-level theories and experimental data. Scaling exponents as a function of degree of polymerization are extracted. The distribution of the end-to-end distance is bimodal for the dimer and gradually shifts to a single peak as the degree of polymerization increases. The scaling exponents for the average chain radius of gyration and end-to-end distance are 0.594 and 0.571, respectively. The values of the heat capacity, isothermal compressibility, and thermal expansivity agree well with the available experimental data, which are of much longer PET chains. The scaling exponents for the self-diffusivity and zero-shear-rate viscosity are, respectively, −2.01 and 0.96, with the latter one being close to the theoretical prediction 1.0 for short-chain polymers.

1. Introduction

Poly(ethylene terephthalate) (PET) is one of the most important engineering plastics and is widely used in bottles, fibers, and packaging films. Industrially, one way to produce PET is through the polycondensation of ethylene glycol (EG) and pure terephthalic acid (PTA). The production process includes two steps. First, PTA is esterified with EG to form a prepolymer consisting of the monomer bis(hydroxyethylene terephthalate) (BHET) and short-chain oligomers (dimer, trimer etc.). Second, the prepolymer is condensed into PET in the melt phase by polycondensation. Clearly, the prepolymer is the bridge between the two steps. Therefore, understanding the thermodynamic and transport properties of the monomer and oligomers will help in the modeling of finishing reactors. For example, to understand the temperature profile in the reactor, it is necessary to know the heat capacities and thermal conductivities of the components. However, these physical properties are not available currently and could be obtained either by experiments or by computer simulation techniques.

The macroscopic structure/property relationships of PET and their composites have been well understood by researchers through experiments, while the experimental work on that of PET monomers and oligomers is rare.[1,2] One reason for scarcity of oligomer data is that, experimentally, it is difficult to trace the initial polymerization process and separate the oligomers under reaction state point and often unsafe for sampling during reaction.[3,4] An alternative way to generate these physical properties is through molecular simulation.

The bulk properties of polymers have molecular origins, which can be revealed through molecular simulation. In addition to simply providing a property data point as a function of polymer architecture, molecular simulations can also provide insight into the structural changes ultimately responsible for the behavior. For example, molecular simulations have shown how polyethylene molecular weight impacts shear and extensional viscosities.[5−7] As another example, molecular simulations have shown how changes in the backbone architecture of perfluoropolyethers impact rheological properties.[8,9] In addition, molecular simulation is able to provide insight into the formation of intermolecular and intramolecular hydrogen bonding though corresponding pair correlation functions,[10,11] which is helpful in understanding the microstructure and macroscopic properties of materials. Consequently, molecular simulation can provide a useful path for the determination of the physical properties (thermodynamic, transport, and structural) of PET oligomers as a function of degree of polymerization. A detailed and systematic atomistic understanding of PET oligomers can contribute to the optimization of the operation of finishing reactors.

PET has previously been studied via molecular simulation. Hedenqvist et al.[12] developed an atomistic model for PET (hereafter referred to as the HBB model) and studied the PVT and structure behavior of PET chains. The specific volume, solubility parameters, and dipolar correlation factors obtained from molecular dynamics (MD) simulation are in good agreement with the experimental results. Implementing the HBB model for PET in MD simulations, Bharadwaj[13] further studied the diffusion of methane in amorphous PET and other two aromatic polyesters and investigated the diffusion coefficients of PET in the temperature ranges of 450−625 K. Boyd et al. modified the torsion component of the HBB potential to satisfy chain dynamics and relaxation.[14] Using the modified HBB model, Kamio et al.[15] performed atomistic simulations of PET dimers and decamers to derive a coarse-grained model for long PET chain molecules. Other models used in the molecular

* Author to whom correspondence should be addressed. E-mail: dkeffer@utk.edu. Telephone: (865)-974-5322.
† University of Tennessee.
‡ Eastman Chemical Company.

MD Simulation of PET Oligomers

J. Phys. Chem. B, Vol. 114, No. 2, 2010 **787**

simulation of PET include the polymer consistent force field (PCFF) model to study the structural, conformational, dynamic, and barrier properties of the amorphous (glassy and melt) phases PET and PEI [poly(ethylene isophthalate)] by Karayiannis et al.[16] The open force field (OFF) model was used to study diffusion of O_2 and CO_2 in PET and related alkylene and isomeric polyesters reported by Shanks and Pavel.[17] The rotational isomeric state (RIS) conformational model was used to study PET chain conformation and relaxation by Cail et al.,[18] conformational and elastic behavior of PET network by Saunders et al.,[19] and conformational characteristics of PET and PEI by Tonelli.[20]

Compared to long chains of PET, the simulation work on PET oligomers is limited. Cho[21] studied the formation of cyclic oligomers by ester interchange reaction in PET through the Monte Carlo method on the basis of the rotational isomeric state (RIS) model. Using the same model, Aoki[22] reported that neighboring phenyl−phenyl ring interactions enhance the probability of small end-to-end distances based on the conformational analysis of a linear trimer of PET. Recently, West et al.[2] did a similar conformational analysis on the PET dimer and justified the presence of a low-energy conformation involving hydrogen bonding between the terminal hydroxyl and the carbonyl, which is given as the reason for low reactivity of the dimer compared with other oligomers.

In this work, we performed a systematic set of molecular dynamic simulations of PET oligomers in the isobaric−isothermal (NpT) ensemble. We studied thermodynamic properties (density, potential energy, enthalpy, heat capacity, isothermal compressibility, and thermal expansivity), transport properties (self-diffusivity, zero-shear-rate viscosity, thermal conductivity), and structural properties (pair correlation functions, hydrogen bonding network, end-to-end chain distance) as a function of degree of polymerization from 1 to 10 repeat units. This paper is organized as follows. The details on the potential and simulation techniques are given in section 2. The results and discussion are presented in section 3. The conclusions are listed in section 4.

2. Simulation Method

We use the anisotropic united atom HBB potential model developed by Hedenqvist, Bharadwaj, and Boyd[12,14] for PET to describe the intramolecular and intermolecular potential of BHET and oligomers molecules. All atoms of the PET oligomer molecule are explicitly represented except for the hydrogen bound to carbon. The intramolecular interaction includes bond stretching, bond bending, bond torsion, and bond out-of-plane bending, and electrostatic and Lennard-Jones interactions, intramolecular electrostatic, and Lennard-Jones interactions are counted for sites separated by at least four bonds. Intermolecular interactions are described by electrostatic and Lennard-Jones potentials. All the parameters are from Hedenqvist et al. except for the partial charges for the end −OH group, which are thus taken from the alcohol work of Chen et al.[23] The hydrogen in the −OH group is the only explicit hydrogen in the model. It is important to have an explicit O and H in the alcohol group in order to observe hydrogen bonding. See Figure 1 for a schematic of the molecule.

For the evaluation of the electrostatic energy, we use the spherically truncated charge-neutralized method developed by Wolf et al.[24] The electrostatic and Lennard-Jones interactions are truncated at a cutoff distance of 15 Å.

We simulated in the isobaric−isothermal (NpT) ensemble since the industrially relevant state points of interest are defined
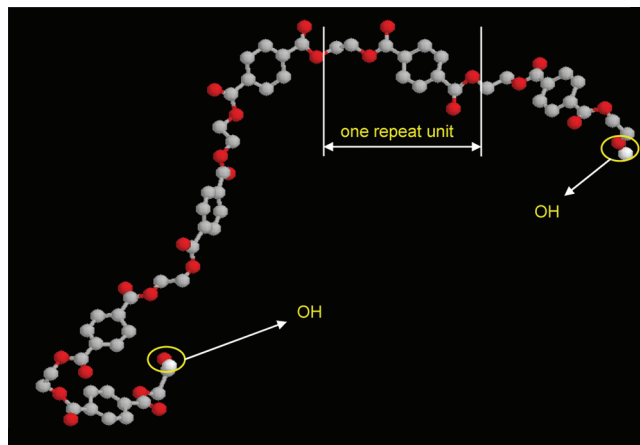

Figure 1. Model of the PET hexamer molecule, showing a repeat unit. The only explicit hydrogens are those in the terminal alcohol group.

by pressure (*p*) and temperature (*T*). We implemented the Hamiltonian-based thermostat and barostat of Keffer et al.[25,26] Both the thermostat and barostat frequencies were set to 10^{-4} fs. We used the XI-RESPA NPT algorithm developed by Tuckerman et al.[27] to solve the equation of motion. The large time step is 2 fs, and the small time step is 0.2 fs.

The parallel code we used was built in-house and is written in FORTRAN-90, using MPI for interprocessor communication. It has been tested rigorously across a variety of applications. For the simulations in this work, we verified conservation of the Hamiltonian in order to validate our choices of time step and cutoff distance and to minimize the possibility of bugs in the potential. The simulations are executed on 16 nodes. The wall-clock time required for the execution of 1 ns of simulation is about a day for DP = 1 (216 molecules) and a week for DP = 10 (125 molecules) systems. Thus, to finish a run of 30 ns for DP equals 10, it took roughly 6 months.

For degrees of polymerization (DP) of 1, 2, and 3, we simulated 216 molecules. For DP from 4 to 10, we simulated 125 molecules. The state point was set at 0.13 kPa and 563 K, as this corresponds to conditions within a finishing reactor.[28] As for the initial conditions, we estimated the initial density and placed the particles in the simulation volume, avoiding significant overlap. We equilibrated the particle positions first, keeping the density and temperature constant. Then we performed a second equilibration in which the thermostat and barostat were activated and the system equilibrated to the correct density. Typically, this equilibration lasted for 1 ns. Data production followed and lasted from 1 ns for the monomer to over 30 ns for the octamer and decamer. These lengths of data production were chosen to be greater than the longest rotational relaxation time as determined in the simulation.

3. Results and Discussion

In this section, we present the results of the MD simulations for the full set of degrees of polymerization, DP = 1, 2, 3, 4, 6, 8, and 10, in three sections: structural properties, equilibrium thermodynamic properties, and transport properties. A summary of the properties generated from the simulations is presented in Table 1.

3.1. Structural Properties. In Figure 2, we show snapshots from the MD simulations. All of the simulated systems correspond to dense liquids. For the purposes of visualization of the individual chain conformations, we render all but a few of the chains invisible in the snapshots b through f. Compare

TABLE 1: Simulation Data for DP = 1, 2, 3, 4, 6, 8, and 10 at p = 0.13 kPa, T = 563 K

DP	1	2	3	4	6	8	10
N	216	216	216	125	125	125	125
V (10^5 Å^3)	0.70 ± 0.04	1.21 ± 0.06	1.71 ± 0.03	1.28 ± 0.01	1.87 ± 0.01	2.46 ± 0.01	3.06 ± 0.01
ρ (g/cm^3)	1.30 ± 0.01	1.26 ± 0.01	1.28 ± 0.02	1.29 ± 0.01	1.29 ± 0.01	1.29 ± 0.01	1.29 ± 0.01
U (10^2 aJ)	−0.15 ± 0.01	0.20 ± 0.05	1.26 ± 0.03	1.39 ± 0.05	3.38 ± 0.17	5.44 ± 2.03	7.43 ± 4.06
H (10^2 aJ)	−0.15 ± 0.01	0.20 ± 0.05	1.26 ± 0.03	1.38 ± 0.05	3.38 ± 0.17	5.44 ± 2.03	7.43 ± 4.06
C_p (10^3 J/K/kg)	2.73 ± 0.09	2.56 ± 0.06	2.47 ± 0.06	2.45 ± 0.07	2.35 ± 0.05	2.29 ± 0.04	2.25 ± 0.05
β (10^{-1} GPa^{-1})	2.17 ± 0.77	3.02 ± 1.12	4.70 ± 3.27	4.51 ± 1.65	3.44 ± 0.44	6.40 ± 3.06	5.21 ± 4.43
α (10^{-4} K^{-1})	6.73 ± 1.02	5.26 ± 0.38	4.81 ± 0.55	4.80 ± 0.17	4.53 ± 0.27	4.28 ± 0.16	3.75 ± 0.79
D (10^{-10} m^2/s)	5.68 ± 1.14	2.05 ± 0.23	0.71 ± 0.14	0.40 ± 0.09	0.17 ± 0.02	0.10 ± 0.03	0.07 ± 0.01
η (10^{-2} Pa·s)	0.27 ± 0.01	0.55 ± 0.08	0.58 ± 0.09	0.65 ± 0.07	1.95 ± 0.65	2.23 ± 0.60	3.03 ± 0.80
v_s (10^3 m/s)	2.01	1.75	1.39	1.41	1.62	1.18	1.31
λ_{GK} (W/m/K)	0.16	0.16	0.13	0.14	0.16	0.12	0.13
λ_B (W/m/K)	0.21 ± 0.02	0.20 ± 0.05	0.31 ± 0.02	0.13 ± 0.11	0.12 ± 0.07	0.22 ± 0.03	0.18 ± 0.01
H-bond (2.0 Å) (%)	54.22	42.72	42.57	38.84	28.55	22.25	20.55
H-bond (2.5 Å) (%)	69.50	57.16	55.11	51.02	38.01	30.18	27.44
$\langle R_{ete} \rangle$ (Å)	9.8 ± 1.0	13.6 ± 4.9	18.3 ± 6.6	21.1 ± 7.5	26.8 ± 10.2	28.6 ± 11.2	34.2 ± 9.4
$\langle R_g \rangle$ (Å)	4.0 ± 0.7	5.6 ± 2.8	7.6 ± 2.7	8.9 ± 5.2	11.2 ± 4.4	12.5 ± 5.3	13.2 ± 3.8
R_{SE} (Å)	4.06	5.54	14.96	23.70	19.23	28.02	31.9
T_R (ns)	0.128	0.552	2.42	5.59	15.26	27.8	37.5
T_{KWW} (ns)	0.129	0.502	2.81	5.59	15.78	25.3	38.6
β_{KWW}	0.98	0.92	0.76	0.76	0.77	0.77	0.74

for example, the monomer snapshots in Figure 2a, in which all molecules are shown, and Figure 2b, in which only a few are shown. We will refer back to this figure in the discussion of the structural properties below.
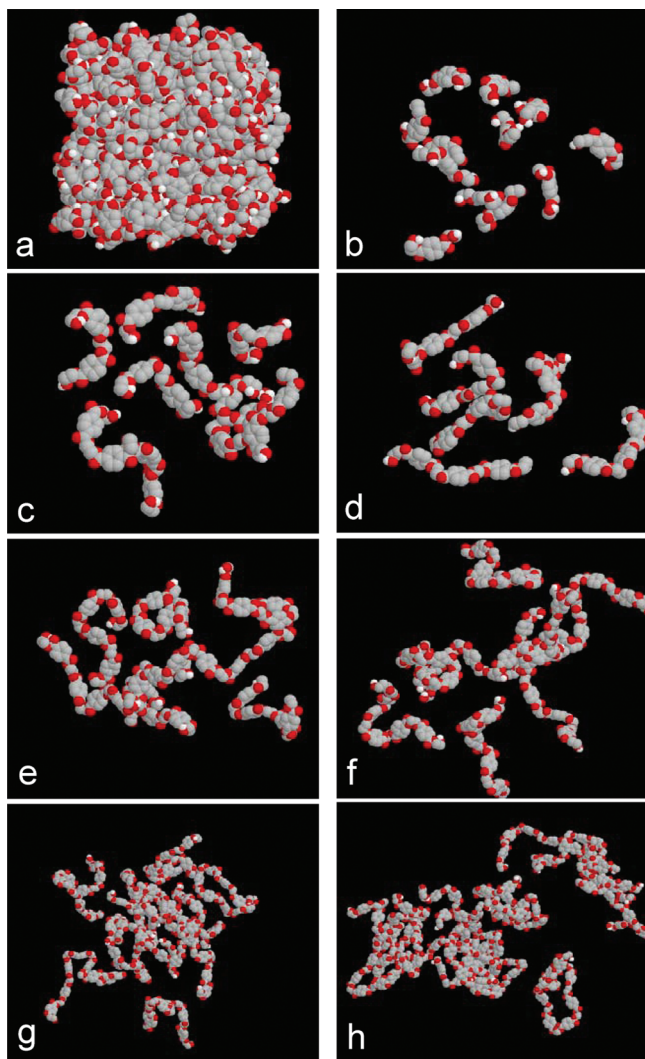

Figure 2. Snapshots of equilibrium configurations from simulations at T = 563 K, p = 0.13 kPa: (a) monomer, all molecules shown; (b)−(h) oligomers, selected molecules; (b) monomer; (c) dimer; (d) trimer; (e) tetramer; (f) hexamer; (g) octamer; (h) decamer.

In Figure 3, we show the distribution of chain end-to-end distance for the full set of DPs studied in this work, DP = 1, 2, 3, 4, 6, 8, and 10. The end-to-end distance is defined as the distance between the carbons attached to the terminal alcohol groups. The end-to-end distance for the monomer shows a single peak centered at 9.8 Å, as expected since the monomer is relatively inflexible. In Figure 2b, we show a snapshot of selected monomer molecules, all of which have very similar end-to-end distances. The end-to-end curve of the dimer displays two peaks, one on either side of the monomer peak. The peak centered at 4.5 Å corresponds to a folded configuration, as shown in Figure 2c. The broader peak extending from 7 to 22 Å, with a maximum at 16.2 Å, corresponds to the unfolded conformation. These two peaks in the end-to-end distance distribution of the PET dimer molecule have also been reported by West.[2] As the DP of polymerization increases, the qualitative two-peak behavior of the dimer is still observed, but the magnitude of the first peak diminishes. Also, the distance at which the maximum in the second peak occurs increases with DP, and the breadth of the curve increases with DP. The average end-to-end distance increases with DP, as can be seen in Table 1.

In Figure 4, we plot the average end-to-end distance and the average radius of gyration as a function of DP on a log−log plot. In order to determine scaling exponents, we fit these data to an equation of the form
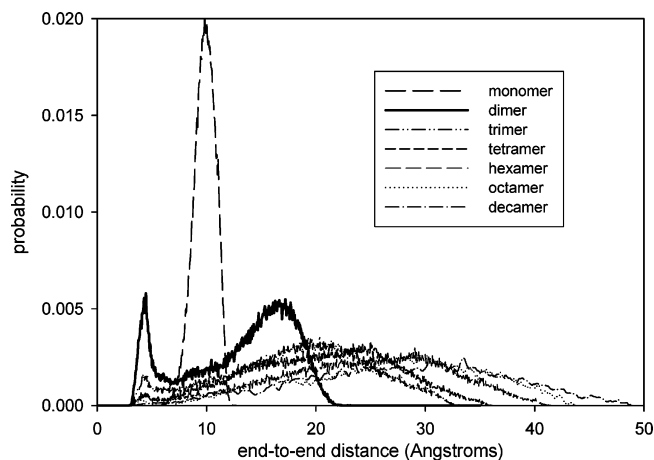

Figure 3. Chain end-to-end distance distributions as a function of degree of polymerization (DP).

MD Simulation of PET Oligomers

J. Phys. Chem. B, Vol. 114, No. 2, 2010 **789**

$$X = a(DP)^b \qquad (1)$$

where X is a property related to DP via the scaling exponent, b. Both structural measures can be well fitted by eq 1. The scaling exponents for the radius of gyration and the chain end-to-end distance are 0.594 and 0.571, respectively. These exponents are close to 0.589, which is the scaling exponent for characteristic polymer size in the case of a dilute solution of chains in a good solvent, where the chains behave as self-avoiding walks (SAWs).[29] In a melt of sufficiently long PET chains, chains should behave as random walks and the exponent should be close to 0.5 as shown by Kamio et al.[15] That our chains display scaling behavior closer to the dilute solution limit is an indication of the fact that our chains are too short to display the behavior of an entangled polymer melt. Furthermore, Laso and Karayiannis[30,31] studied scaling laws of freely joint chain systems under various packing densities. Very similar values (0.58−0.60) for scaling exponents are obtained for short chains in the whole range of volume fractions from dilute up to very dense samples, and the departure from the Gaussian coil concept is attributed to the short chain length studied, suggesting a universal character in the scaling behavior of oligomers.

In addition to the distribution of the chain end-to-end distance, we can extract useful information from the dynamics of the end-to-end vector autocorrelation function. In Figure 5, we plot the end-to-end vector autocorrelation function as a function of
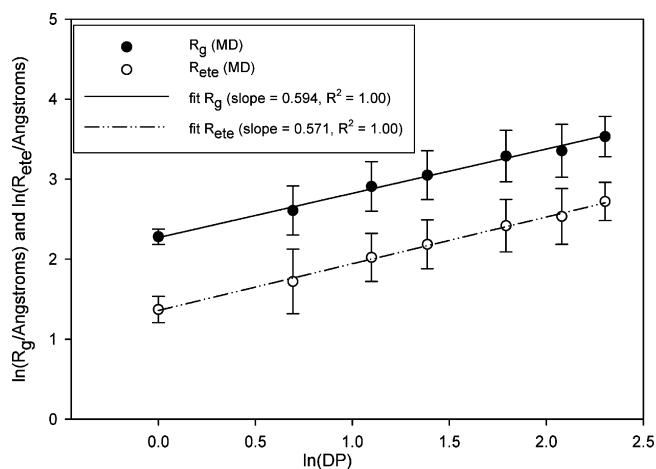

Figure 6. Intermolecular oxygen−hydrogen pair correlation function as a function of DP.

Figure 4. Average chain end-to-end distance (R_{ete}) and chain radius of gyration (R_g) as a function of DP.
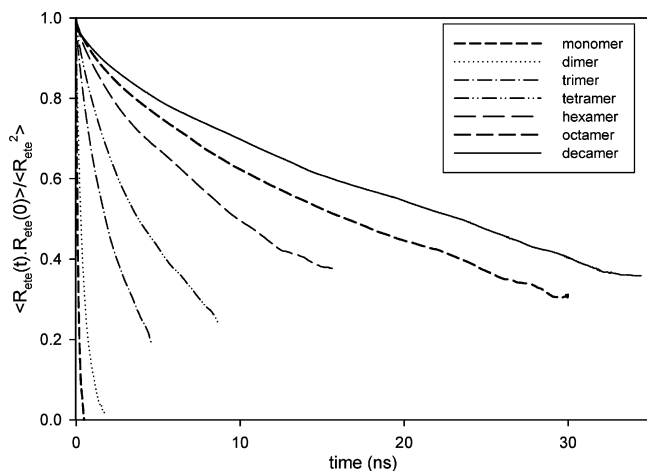

Figure 5. Chain end-to-end distance (R_{ete}) autocorrelation functions as a function of observation time for all DPs studied.
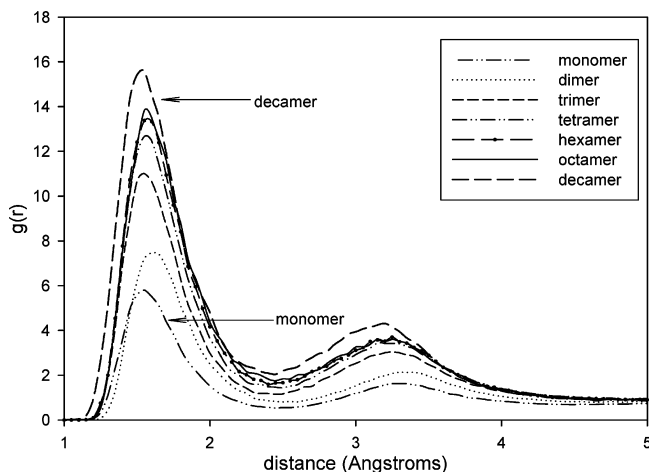
elapsed time for all DPs studied. Each curve is normalized such that it is unity at the origin. By fitting this data to the Rouse model (a simple exponential) or the KWW model[32] (a stretched exponential), one can extract chain relaxation times, τ_R and τ_{kww}, respectively. These times correspond to the longest rotational relaxation time. The relaxation times are reported in Table 1. The stretching exponent, β_{KWW}, is also reported in Table 1. The fits are reasonably good. When viewed on a log axis (see the Supporting Information), there is evidence of deviation from the fits at very short times, which may hint at a different mechanism for the initial relaxation, corresponding to decorrelation events specific to PET chemistry. The relaxation times from the Rouse and the KWW model agree relatively well. The relaxation times increase strongly with DP. The scaling exponent b for τ_{kww} is 2.78. We note that our oligomers are too short to be entangled and our simulation time is not long enough to see a Rouse scaling,[32] for which $b = 2$.

The relaxation times determined above were used to set the duration of the MD simulations. Ideally, we would like the MD simulation to be run for some time significantly longer than the longest relaxation time, in order to average out fluctuations that occur at that longest period. For the simulation of the monomer, when we simulated 1 ns, we were simulating about 8 times longer than the longest relaxation time. As the DP increased, we had to also increase the duration of the simulation. For the octamer and decamer we simulated 30 ns, which is slightly longer than the relaxation time for DP = 8 and slightly shorter than the relaxation time for DP = 10. This limitation imposed by finite computational resources renders the estimation of τ_{kww} less accurate for the longer chains.

Another structural property investigated in this work is the extent of hydrogen bonding. We characterized the hydrogen bonding of the system in terms of the oxygen−hydrogen pair correlation function (PCF) for DP = 1, 2, 3, 4, 6, 8, and 10, as shown in Figure 6. In Figure 6, there are two characteristic peaks of hydrogen bonding; the first is located at approximately 1.8 Å and the second at about 3.3 Å. The first peak corresponds to the distance between the O of one alcohol group and the H in another alcohol group participating in the hydrogen bond. The second peak corresponds to the H and O in each of the alcohol groups that are not participating directly in the hydrogen bond. While it is clear that the number of alcohol groups per repeat unit decreases with DP, the intensity of the peaks increases with DP. This is because the PCF is normalized by the average density of alcohol groups. In other words, the number of alcohol
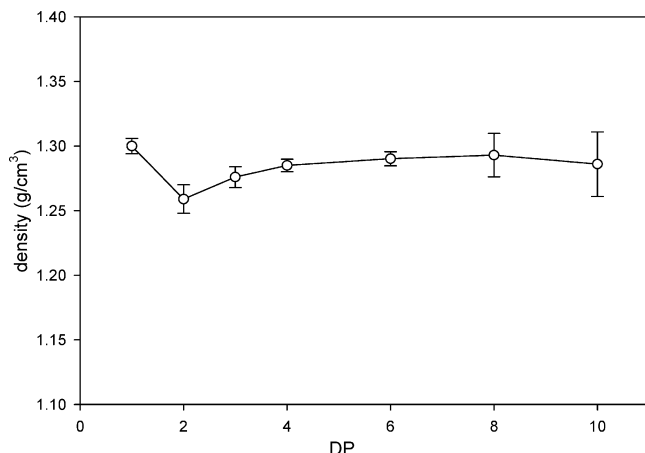
Figure 7. Mass density (ρ) as a function of DP.

Figure 8. Individual nonbonded contributions to the potential energy as a function of DP. ES = electrostatic; LJ = Lennard-Jones; intra = intramolecular; inter = intermolecular. These contributions are normalized by the degree of polymerization.

Figure 9. Enthalpy as a function of DP. The main figure is plotted on a molecular basis. The inset is normalized by DP.

groups decreases with DP, but on a per alcohol basis, the tendency to form hydrogen bonds increases. In Table 1, we report some statistics describing the hydrogen bonding network as a function of DP. The hydrogen bond fraction is the percentage of OH groups involved in hydrogen bonding, being calculated through the integration of the oxygen−hydrogen pair correlation functions (Figure 6), and we see that the percentage of OH involved in hydrogen bonding decreases with DP, which is mainly because the number density of OH groups decreases with increasing chain length.

3.2. Thermodynamic Properties. The melt density, potential energy, enthalpy, heat capacity, isothermal compressibility, and thermal expansivity at 0.13 kPa and 563 K have been calculated from the MD simulations. All of these thermodynamic properties are listed in Table 1. In this section, we discuss the properties individually and compare to experiment, where possible.

Figure 7 shows the density changing as a function of DP. The densities of PET oligomers obtained from the simulations are near 1.3 g/cm^3. There is a literature value for the monomer density, but it is at the state point of 293 K and 1 atm, rather than the state point chosen to model the interior of the finishing reactor. Therefore, we also ran a simulation of the monomer at 293 K and 1 atm to provide a validation of the density predictions of our model. The density of the monomer at 293 K and 1 atm from simulation is 1.313 ± 0.02 g/cm^3, which can be compared with the reported value of 1.315 ± 0.06 g/cm^3 from the CAS database (#959-26-2). The difference is within 0.2%.

We observe that the simulation value of the oligomers is higher than that of PET and it is not sensitively changing with DP, because of the hydrogen bonding in the oligomer system. For reference, we show the melt density of PET is around 1.2 g/cm^3 (under $p = 1$ atm, $T = 563$ K).[33]

In Figure 8, the nonbonded contributions to the potential energy are plotted as a function of DP on a per DP basis. (The number of nonbonded contributions fluctuates during the simulation and makes reporting on a per mode basis less useful.) All nonbonded interactions are negative (attractive) as the reference state (zero energy) for these interactions is infinite separation, and the pressure is not sufficiently high to force repulsive energies. Intuitively, as the chain length increases, one expects intramolecular interactions to increase in magnitude and intermolecular interactions to decrease in magnitude since a given atom will be on average interacting with a greater fraction of molecules of its chain. The total intermolecular interaction does indeed follow the intuitive understanding that, as DP increases, the magnitude decreases. However, the total intramo-
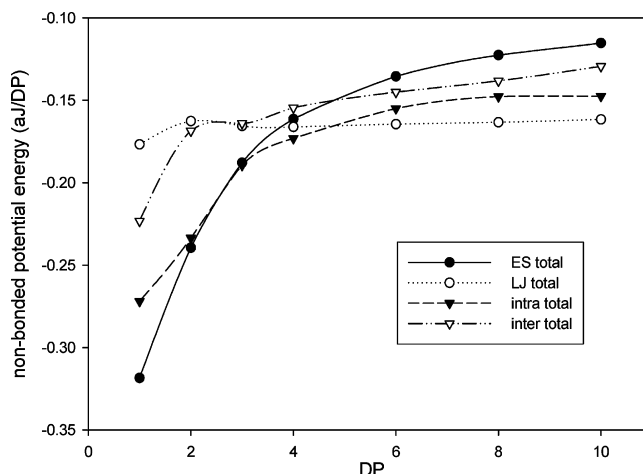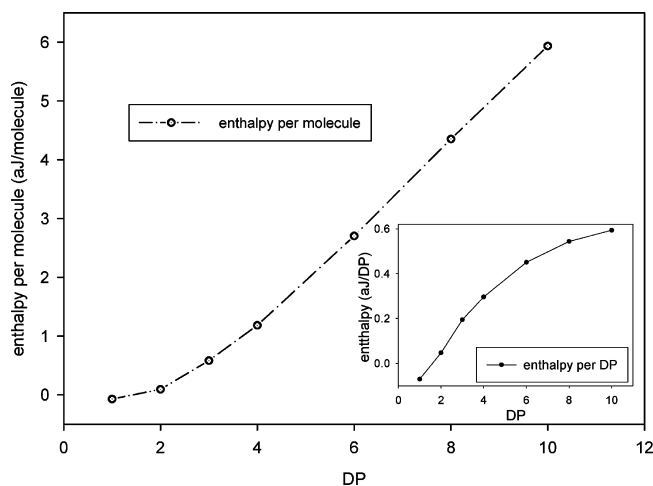
lecular interaction also decreases, which is somewhat counterintuitive until one considers hydrogen bonding. The end groups of the chain form hydrogen bonds. As the chain length increases, the relative number of end groups per DP decrease. Therefore, we see a decrease in the electrostatic contribution to the potential energy on a per DP basis. Some portion of the electrostatic energy is due to intramolecular interactions. Apparently, the loss of intramolecular electrostatic interactions is sufficient to overwhelm the other gains in intramolecular interactions, resulting in a total intramolecular interaction that decreases in magnitude with DP, but not quite as quickly as the electrostatic term.

The enthalpy is composed of a kinetic energy term, a potential energy term (which together constitute the internal energy), and a pV term. In Figure 9, we plot the enthalpy per molecule as a function of DP on both a per molecule basis and on a per DP basis (inset). The enthalpy approaches a linear behavior with respect to DP at large DPs, as expected since the kinetic energy and potential energy should scale roughly linearly with DP when the change in density, accounted for by the pV term, is relatively small. The pronounced deviation from linearity at low DP is due to the fact that the end groups are slightly different than the repeat units in the interior of the chain. The slight deviation from linearity at high DP is better seen on a per DP basis and

TABLE 2: Comparison of Thermodynamic Properties from Finite Difference and Fluctuation Methods for the Monomer at T = 563 K and p = 100 atm[a]

thermodynamic properties	MD (fluctuation)	MD (finite difference)	experimental data (PET)
heat capacity (10^3 J K^{-1} kg^{-1})	1.41 ± 1.38	2.68 ± 0.08	2.66^{35}
isothermal compressibility (10^{-1} GPa^{-1})	17.61 ± 10.20	3.14 ± 0.06	3.24^{36}
thermal expansion coefficient (10^{-4} K^{-1})	21.40 ± 19.71	6.42 ± 0.96	6.55^{35}

^{a} As a reference point, experimental values for PET are also provided.

is largely accounted for by the nonbonded contributions to the potential energy shown in Figure 9.

Thermodynamic properties that correspond to partial derivatives, such as the constant-pressure heat capacity, C_p, the isothermal compressibility, β, and the thermal expansivity, α, can be calculated from statistical thermodynamics based on fluctuations in the NpT ensemble.[34] The constant pressure heat capacity is proportional to the variance of the enthalpy

$$C_p = \frac{1}{Vk_BT^2}\langle\sigma_H^2\rangle \qquad (2.a)$$

The isothermal compressibility is obtained through the variance of volume

$$\beta = \frac{1}{Vk_BT}\langle\sigma_V^2\rangle \qquad (2.b)$$

The thermal expansion coefficient is based on the covariance of volume and enthalpy of the

$$\alpha = \frac{1}{Vk_BT^2}\langle\sigma_{(V)(H)}\rangle \qquad (2.c)$$

where V is the volume, T is the temperature of the system, and k_B is Boltzmann's constant. The angled brackets indicate an ensemble average. These fluctuations provide an elegant method to obtain these thermodynamic properties, since we can obtain all these three properties from one single MD simulation at the desired state point.

For reasons that will be made clear shortly, we also calculated C_p, β, and α using a second procedure, namely, centered finite difference. In this approach, one runs three simulations for each thermodynamic property. For example, for the heat capacity, one runs a simulation at the state point defined by (p,T), then two other simulations at $(p, T + \varepsilon)$ and $(p, T - \varepsilon)$. The choice of ε is made so that one can observe statistically valid differences in the enthalpy between the state points. Thus the heat capacity can be determined as

$$C_p = \frac{H(p, T + \varepsilon) - H(p, T - \varepsilon)}{2\varepsilon} \qquad (3.a)$$

Similarly, the isothermal compressibility and thermal expansivity can be expressed as

$$\beta = -\frac{1}{V(p,T)}\frac{V(p + \varepsilon, T) - V(p - \varepsilon, T)}{2\varepsilon} \qquad (3.b)$$

$$\alpha = \frac{1}{V(p,T)}\frac{V(p, T + \varepsilon) - V(p, T - \varepsilon)}{2\varepsilon} \qquad (3.c)$$

In Table 2, we report C_p, β, and α for the monomer at a state point of 10 MPa and 563 K.[35] We choose this state point rather than the one corresponding to the interior of the finishing reactor, which has been used in all other simulations, in order to compare with experimental data. We see that using the finite difference approach yields better mean values in agreement with experimental data for PET[35,36] and yields much smaller uncertainties, showing that the simulation results are reasonable (exact
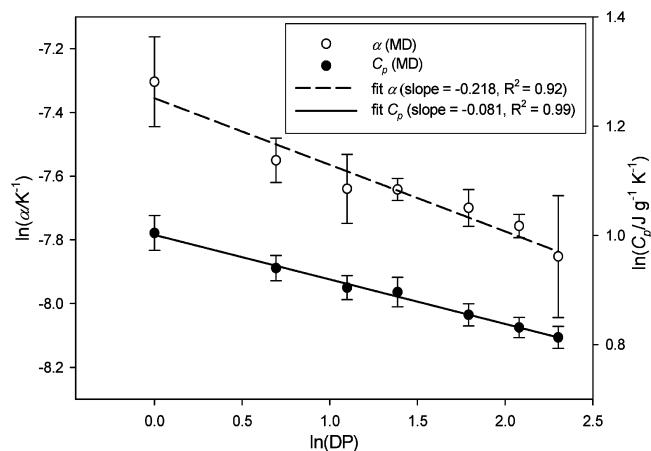

Figure 10. Heat capacity (C_p) and thermal expansivity (α) as a function of DP. The fits are to eq 1. The R^2 measure of fit is also reported in the legend.

agreement with experimental data was not expected due to the difference in DP) and the method is statistically reliable. The uncertainties from the quantities obtained from the fluctuations in some cases approach 100%. These uncertainties were calculated by dividing the simulation into 10 blocks of time, computing the average heat property in each block, and computing the corresponding standard error in the block average. In Table 1, we report the values of C_p, β, and α using the centered finite difference formulas as a function of DP at the finishing reactor state point. The uncertainties for β are larger than the uncertainties for C_p and α because β is based upon simulations run at different pressures, whereas C_p and α are based upon simulations run at different temperatures, and the greater fluctuations in the pressure increase the uncertainty of the resulting finite difference.

In Figure 10, we show the dependence of C_p and α on DP on a log–log plot. The heat capacity on a per mass basis decreases with DP. The thermal expansivity also decreases with DP. Both of these trends have been observed experimentally.[37] We extracted scaling exponents for C_p and α of -0.081 and -0.218, respectively. We do not report a scaling exponent for β due to increased uncertainty in this property for reasons mentioned above.

In the simulations, the hydrogens attached to the carbon are not modeled explicitly. Thus the contributions to the thermodynamic properties, including the heat capacity, due to the high-frequency C–H vibrations are not included. Thus we underestimate the heat capacity. For methane at room temperature, the vibrational modes contribute less than 10% to the heat capacity, and this serves as an extreme limit on the underestimation.[38]

3.3. Transport Properties. One can obtain transport properties from equilibrium simulations using Green–Kubo relations.[39–41] In this work, we report the self-diffusivity (D), zero-shear rate viscosity (η), and thermal conductivity (λ) as a function of DP. The self-diffusivity is obtained from the mean-square displacements (MSD) through Einstein's equation given as

$$\mathbf{D} = \frac{1}{6}\lim_{t\to\infty}\frac{1}{t}\langle[\mathbf{r}_{cm}(t) - \mathbf{r}_{cm}(0)]^2\rangle \qquad (4)$$

where $\mathbf{r}_{cm}$ is the center of mass position of the molecule.

For the case of the self-diffusivity, this integral can also be expressed in terms of the mean square displacement via the Einstein relation. In Figure 11, we plot the mean square displacement versus observation time on a log–log plot. In order to satisfy the infinite time limit, the slopes of the curves must be unity. These slopes are reported in the legend of Figure 11 and are all very close to unity. This is evidence that the simulations have been run sufficiently long to achieve valid self-diffusivities. The numerical values of the self-diffusivities are reported in Table 1 and plotted in Figure 12 as a function of DP. The self-diffusivity decreases with DP as expected. The scaling exponent for the self-diffusivity is −2.01.

The zero-shear-rate viscosity is based on time integration of the momentum autocorrelation function

$$\eta_{xy} = \frac{1}{Vk_BT}\int_0^\infty \langle\sigma_{xy}(t)\,\sigma_{xy}(0)\rangle\,\mathrm{d}t \qquad (5)$$

where σ_{xy} is the xy component of the stress tensor defined to have a potential and kinetic contribution

$$\sigma_{xy} = \frac{1}{2}\sum_{i=1}^N\sum_{j\neq i}^N F_{ijx}r_{ijy} + m_i\sum_{i=1}^N u_{ix}u_{iy} \qquad (6)$$

where r_{ijx} and F_{ijx} are, respectively, the separation and force between particles i and j in the x dimension and m_i is the mass of particle i.

The momentum autocorrelation functions are shown in Figure 13. The autocorrelation functions decay to zero in an oscillatory manner. There is one interesting feature in Figure 13, as is clear in the inset: the magnitude of the oscillations decreases as DP increases. While the correlations may appear to have died out in less than 4 ps, we will see that this is not the case.

In Figure 14, we plot the zero-shear-rate viscosity as a function of the upper limit of integration in eq 5. Following a previously tested procedure,[42] we then average the values of the viscosity that occur on the plateau. The arrows in Figure 14 indicate where we decided the plateau began. In general, the start of the plateau increases with DP. For some DP, the plateau begins long after the 4 ps period in which the autocorrelation functions appear to have died out based on visual inspection of Figure 13. Therefore, fluctuations in the autocorrelation functions beyond about 4 ps are not statistical noise. Nevertheless, for bigger DP, we do see the beginning of the plateau well before an observation time of τ_{KWW}. (We cannot
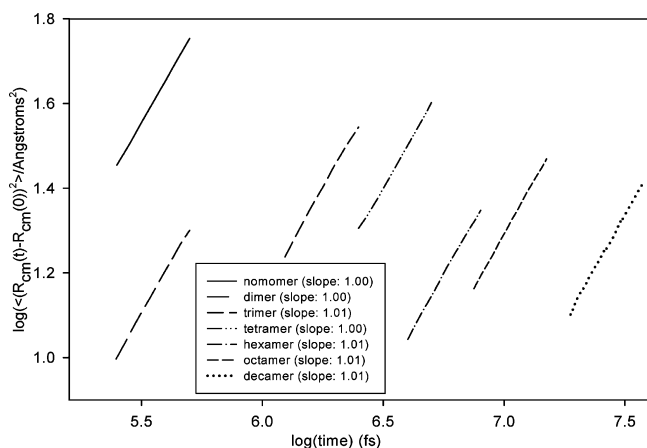

Figure 11. Mean square displacement of chain center of mass as a function of observation time for all DPs. The slope reported in the legend should be unity to satisfy the long-time limit of the Einstein relation.
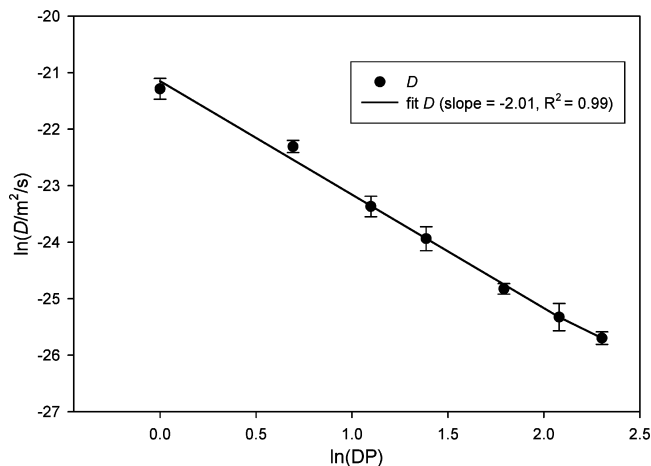

Figure 12. Self-diffusivity (D) as a function of DP.
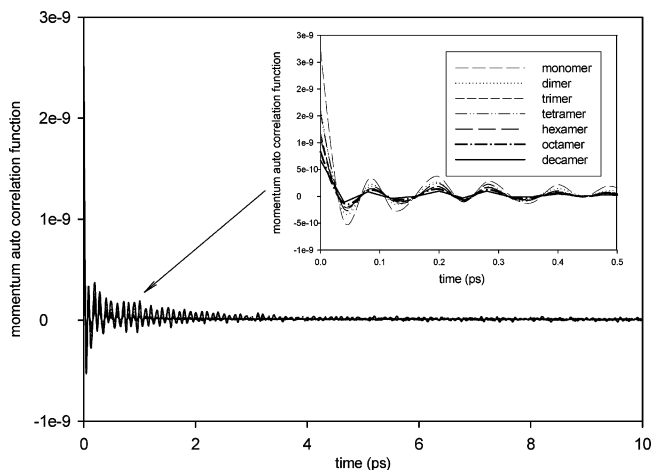

Figure 13. Momentum autocorrelation functions as a function of observation time for all DP. The inset is a close-up of short-time behavior.

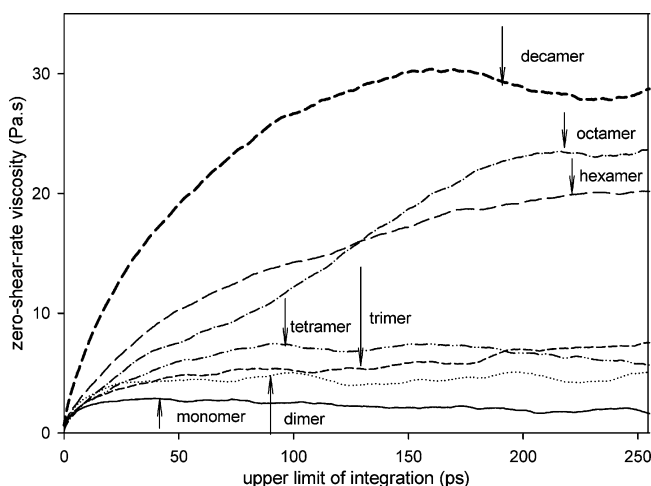**Figure 14.** Zero-shear-rate viscosity (η) as a function of the upper limit of integration in eq 5. The arrows indicate the observation time at which a plateau begins.
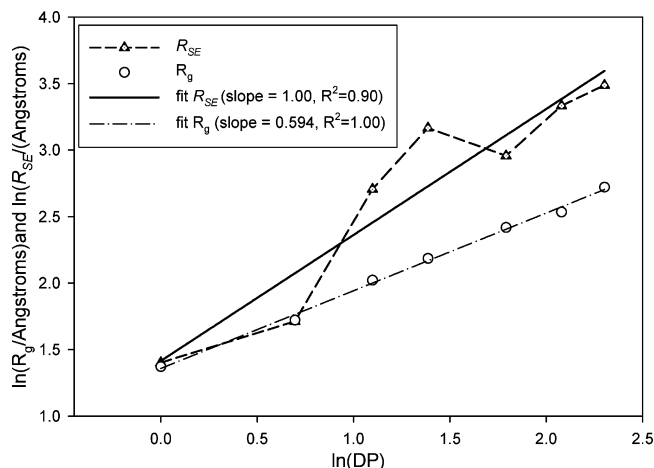
MD Simulation of PET Oligomers

J. Phys. Chem. B, Vol. 114, No. 2, 2010 **793**

Figure 15. Radius of gyration (R_g) and particle radius from the Stokes−Einstein relation (R_{SE}) as a function of DP.

evaluate the autocorrelation function for observation times up to τ_{KWW} for long chains due to the decreasing statistical reliability with increase in observation time.) The implication is that long-time-scale relaxation modes impact the zero-shear-rate viscosity only nominally. The numerical values of the zero-shear-rate viscosities are given in Table 1. The scaling exponent for the zero-shear-rate viscosity is 0.96, which is in agreement with the theoretical value of 1 for short chains.[29]

With both the self-diffusivity and zero-shear-rate viscosity in hand, we can test the Stokes−Einstein (SE) relation,[43,44] which according to hydrodynamic theory applies well to the diffusion of large spherical molecules in solvent of low molecular weight

$$\frac{D\eta}{k_B T} = \frac{1}{4\pi R_{SE}} \qquad (7)$$

where R_{SE} is the particle size. We can use the SE relation to calculate particle size based upon the self-diffusivity and zero-shear-rate viscosity reported above. In Figure 15, we plot on a log−log scale the radius from the SE relation and the radius of gyration from MD. We find that for small molecules (monomer and dimer) there is excellent agreement between the particle size predicted by the SE relation and the radius of gyration. For larger molecules, there is a significant variation, presumably because (i) the longer chains violate the assumption of a spherical particle and (ii) the longer chains violate the assumption of a low molecular weight solvent. More details and generalized equations on the relationship between the effective particle's shape and the translational diffusion coefficient can be found in the work of Kröger et al.[45] The scaling exponent for the SE radius is found to be 1.00, which is dictated by the fact that is it determined from the self-diffusivity and zero-shear-rate viscosity with scaling exponents, respectively, of −2.01 and 0.96. The fluctuations around this best fit are presumably due to statistical noise.

The last transport property obtained in this work is the thermal conductivity, λ, which via a Green−Kubo integral can be expressed as a function of an autocorrelation of the heat flux, **J**

$$\lambda = \frac{1}{3Vk_B T^2} \int_0^\infty \langle \mathbf{J}(t) \cdot \mathbf{J}(0) \rangle \, dt \qquad (8)$$

where the heat flux **J** is defined as

$$\mathbf{J} = \sum_{i=1}^{N} u_i E_i + \frac{1}{2} \sum_{i=1}^{N} \sum_{j \neq i}^{N} r_{ij} F_{ij} \cdot u_i \qquad (9)$$

to have contributions from energy carried by a mass flux (the first term) and intermolecular interactions (the second term).

The energy carried by a particle is composed of kinetic and potential contributions.

$$E_i = \frac{1}{2} m_i u_i^2 + \frac{1}{2} \sum_{j \neq i}^{N} U_{ij} \qquad (10)$$

The above atomic heat flux expression has been successfully applied to the systems governed by pair potentials as reported in many articles,[41,46−48] in which the Green−Kubo integral is used to obtain thermal conductivity of small molecules (methane[47] and SiH$_4$[41]). These molecules can be treated as particles by ignoring the intramolecular bond stretching, bond bending, and bond torsion interactions so there will be only intermolecular Lennard-Jones interaction potential contributing to the heat flux. The simulation results based on this procedure are in good agreement with the experimental data. For larger molecules (butane,[49] alkanes[50]), the heat flux expression is often taken as molecular based in order to calculate the molecular heat flux, a heat flux whose description is based on the view that the individual atomic contributions to the local energy density are localized at the molecular centers of mass.[51] This expression applies well to polyatomic molecules with moderate chain length. When the chain length increases, this center of mass based heat flux will be problematic.[52] If the chain is very long, the energy transport along each chain is not ignorable. Therefore, the atomic heat flux expression is needed for prediction of thermal conductivity of polymer chain molecules. Marechal and Ryckaert[53] derived the atomic heat flux expression for polyatomic molecules (n-butane), in which only bond torsion was included, but the thermal conductivity obtained is too large based on experimental comparison with alkanes. An alternative way for faithful prediction of thermal conductivity is to modify the force field or molecular dynamic model. Lussetti et al.[52] transformed the molecule model for poly-amide-6,6 by grouping some atoms in the chain together to have less quantum degree of freedoms in the system as they assume that the high value of thermal conductivity obtained from the MD simulation is due to the incorrect treatment of these fast quantum degrees of freedom in molecular dynamics. They compared the NEMD simulation results of thermal conductivity from different force fields and found that the united atom model with complete rigid bond generated the best result for comparison with the experimental data. Based on the collective conclusions of the work above, we only included nonbonded interactions in the heat flux of our PET oligomer molecules. These nonbonded interactions include both intramolecular and intermolecular Lennard-Jones and electrostatic interactions. Thus, we neglect stretching, bending, and torsion contributions. The heat flux autocorrelation function as a function of DP is shown in Figure 16.

In Figure 17, we plot the thermal conductivity as a function of the upper limit of integration in eq 8. Again, we look for a plateau and report an average beyond the plateau. The data is relatively noisy. We report the numerical values of the thermal conductivities as a function of DP in Table 1. The thermal conductivities of the oligomers fluctuate from 0.12 to 0.30 (W/m/K), which is the reported experimental value range of thermal conductivity for commercial PETs with different crystallinity and molecular weight under 1 atm and 300 K.[33] We plot the thermal conductivity as a function of DP in Figure 18. There is not sufficient statistical reliability in these values to report a scaling exponent (the R^2 measure of fit is 0.04), which in any event would be close to zero.
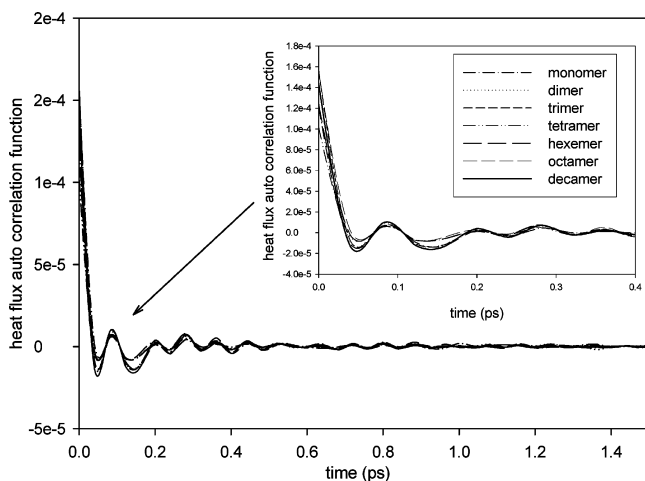
794 *J. Phys. Chem. B, Vol. 114, No. 2, 2010*

Wang et al.

Figure 16. Heat flux autocorrelation functions as a function of observation time for all DP. The inset is a close-up of short-time behavior.
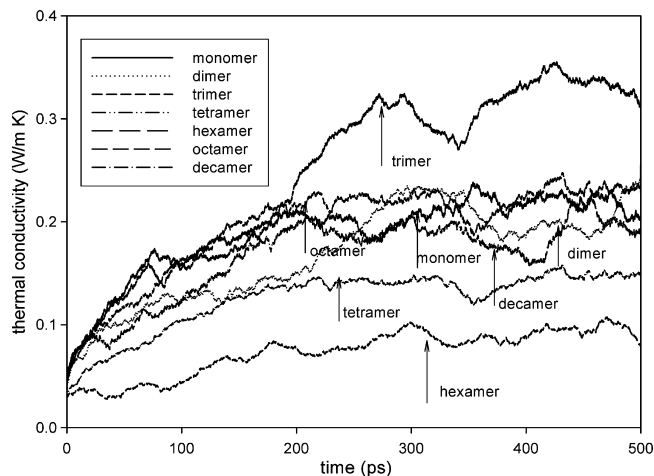

Figure 17. Thermal conductivity (λ) as a function of the upper limit of integration in eq 8. The arrows indicate the observation time at which a plateau begins.
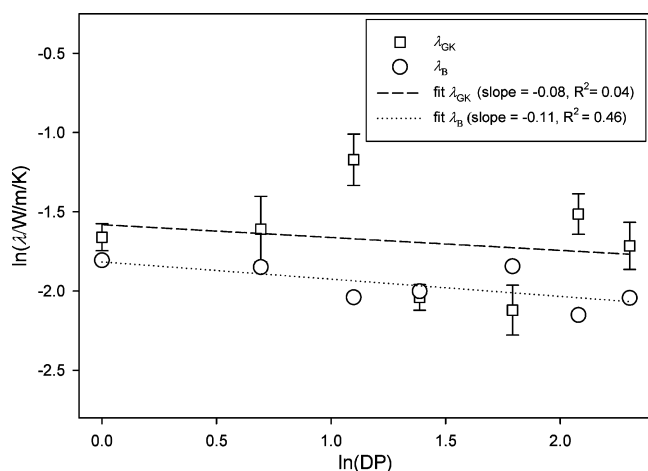

Figure 18. Thermal conductivity obtained from the Green–Kubo integral (λ_{GK}) and the Bridgman equation (λ_B) as a function of DP.

An alternative approach to obtaining the thermal conductivity is to use Bridgman's theory of energy transport in pure liquids.[54,55]

$$\lambda = 3(N/V)^{2/3} k_B v_s \qquad (11)$$

where v_s is the speed of sound in the liquid, given by

$$v_s = \sqrt{\frac{C_p}{C_v}\left(\frac{\partial p}{\partial \rho}\right)_T} \qquad (12)$$

where C_v is the constant volume heat capacity and ρ is the mass density. The partial derivative $((\partial p)/(\partial \rho))_T$ is contained with the isothermal compressibility, which we have already reported. Typically, the ratio of constant-pressure and constant-volume heat capacities is close to unity for liquids. In order to test this assumption, we ran some additional MD simulations on the monomer at constant volume (NVT ensemble) to obtain C_v. We found the ratio to be 1.15, and this is what we used in eq 12 for all DP. The calculated data for velocity of sound is listed in Table 1. It is noted that empirically a coefficient of 2.8 gives a better fit to experimental data than 3 in eq 10,[54] so we used 2.8. The experiments of Bridgman were based on small molecules. Therefore, in eq 11, we used the number density not of chains but of repeat units, which taken independently constitute relatively small molecules. This prediction of the thermal conductivity is also shown in Figure 18. On average the Bridgman thermal conductivity is 26% low. The Bridgman thermal conductivity shows almost a constant with DP (scaling exponent of −0.11), which is similar in the thermal conductivity obtained from the Green–Kubo integral.

4. Conclusions

We obtained structural, thermodynamic, and transport properties for PET oligomers with degrees of polymerization from 1 to 10 at the industrially relevant state point ($T = 563$ K, $p = 0.13$ kPa) by molecular dynamics simulation using a modified HBB model.

The end-to-end distance distribution for oligomers larger than the monomer shows a bimodal distribution in which the chains are either folded or extended. The presence of the folded peak diminishes with DP. The extended peak broadens with DP. The degree of hydrogen bonding, as judged by the fraction of alcohol groups engaged in hydrogen bonding, decreases with DP. The longest rotational relaxation time, radius of gyration, and average end-to-end distance scale with exponents of 2.78, 0.594, and 0.571 respectively.

We generated a suite of thermodynamic properties. We found that both the intramolecular (unexpectedly) and intermolecular (expectedly) nonbonded contributions to the potential energy decrease in magnitude with increasing DP, due to the diminished role of hydrogen bonding in the system. All other contributions on a per mode basis are relatively unaffected by DP.

We compared two methods for obtaining properties based on thermodynamic partial derivatives, such as the heat capacity, isothermal compressibility, and thermal expansivity. The fluctuation method yielded greater statistical uncertainty and poorer agreement with experiment than a method based on using centered finite difference across three simulations. We extracted scaling exponents for C_p and α of −0.081 and −0.218, respectively.

We obtained the self-diffusivity, zero-shear-rate viscosity, and thermal conductivity as a function of DP. The scaling exponents for the self-diffusivity and zero-shear-rate viscosity are, respectively, −2.01 and 0.96. The evaluation of the thermal conductivity from both the Green–Kubo integral and Bridgman theory are both approximate, but yield results that fall in the range of experimental data.

Work is in progress to fit the structural and dynamic information obtained from these atomistic simulations to a coarse-grained model of PET, capable of simulating much larger PET oligomers and polymers.

MD Simulation of PET Oligomers

J. Phys. Chem. B, Vol. 114, No. 2, 2010 **795**

Supporting Information Available: Additional figures supporting our findings in this paper. This information is available free of charge via the Internet at http://pubs.acs.org.

References and Notes

(1) Vermylen, V.; Lodefier, P.; DeVaux, J.; Legras, R.; Mac Donald, W. A.; Rozenberg, R.; De Hoffmann, E. *J. Polym. Sci., Part A: Polym. Chem.* **2000**, *38*, 416.

(2) West, S. M.; Smallridge, A. J.; Uhlherr, A.; Volker, S. *Macromol. Chem. Phys.* **2000**, *201*, 2532.

(3) Amari, T.; Ozaki, Y. *Macromolecules* **2001**, *34*, 7459.

(4) Amari, T.; Ozaki, Y. *Macromolecules* **2002**, *35*, 8020.

(5) Baig, C.; Edwards, B. J.; Keffer, D. J. *Rheol. Acta* **2007**, *46*, 1171.

(6) Baig, C.; Edwards, B. J.; Keffer, D. J.; Cochran, H. D.; Harmandaris, V. A. *J. Chem. Phys.* **2006**, *124*, 084902.

(7) Kim, J. M.; Edwards, B. J.; Keffer, D. J. *J. Mol. Graphics Modell.* **2008**, *26*, 1046.

(8) Jiang, B.; Crawford, N. J.; Keffer, D. J.; Edwards, B. J.; Adcock, J. L. *Mol. Simul.* **2007**, *33*, 871.

(9) Jiang, B.; Kim, J. M.; Keffer, D. J.; Edwards, B. J. *Mol. Simul.* **2008**, *34*, 231.

(10) Ohgi, H.; Sato, T.; Hu, S. H.; Horii, F. *Polymer* **2006**, *47*, 1324.

(11) Martinez, A. G.; Vilar, E. T.; Fraile, A. G.; Martinez-Ruiz, P. *J. Chem. Phys.* **2006**, 124.

(12) Hedenqvist, M. S.; Bharadwaj, R.; Boyd, R. H. *Macromolecules* **1998**, *31*, 1556.

(13) Bharadwaj, R.; Boyd, R. H. *J. Chem. Phys.* **1999**, *110*, 10203.

(14) Boyd, S. U.; Boyd, R. H. *Macromolecules* **2001**, *34*, 7219.

(15) Kamio, K.; Moorthi, K.; Theodorou, D. N. *Macromolecules* **2007**, *40*, 710.

(16) Karayiannis, N. C.; Mavrantzas, V. G.; Theodorou, D. N. *Macromolecules* **2004**, *37*, 2978.

(17) Shanks, R.; Pavel, D. *Mol. Simul.* **2002**, *28*, 939.

(18) Cail, J. I.; Stepto, R. F. T.; Taylor, D. J. R.; Jones, R. A.; Ward, I. M. *Phys. Chem. Chem. Phys.* **2000**, *2*, 4361.

(19) Saunders, L. S.; Ward, I. M.; Cail, J. I.; Stepto, R. F. T. *Polymer* **2004**, *45*, 2357.

(20) Tonelli, A. E. *J. Polym. Sci., Part B: Polym. Phys.* **2002**, *40*, 1254.

(21) Cho, J. S.; Youk, J. H.; Yoo, D. I.; Ko, S. W.; Ha, W. S. *Polym-Korea* **1998**, *22*, 99.

(22) Aoki, A. *Kobunshi Ronbunshu* **1994**, *51*, 283.

(23) Chen, B.; Potoff, J. J.; Siepmann, J. I. *J. Phys. Chem. B* **2001**, *105*, 3093.

(24) Wolf, D.; Keblinski, P.; Phillpot, S. R.; Eggebrecht, J. *J. Chem. Phys.* **1999**, *110*, 8254.

(25) Keffer, D. J.; Baig, C.; Adhangale, P.; Edwards, B. J. *J. Non-Newtonian Fluid Mech.* **2008**, *152*, 129.

(26) Keffer, D. J.; Baig, C.; Adhangale, P.; Edwards, B. J. *Mol. Simul.* **2006**, *32*, 345.

(27) Tuckerman, M.; Berne, B. J.; Martyna, G. J. *J. Chem. Phys.* **1993**, *99*, 2278.

(28) Feldman, D.; Barbalata, A. *Synthetic Polymers: Technology, Properties, Applications*; Chapman & Hall: London, 1996.

(29) Doi, M.; Edwards, S. F. *The Theory of Polymer Dynamics*; Oxford University Press: New York, 1986.

(30) Laso, M.; Karayiannis, N. C. *J. Chem. Phys.* **2008**, *128*, 174901.

(31) Karayiannis, N. C.; Laso, M. *Macromolecules* **2008**, *41*, 1537.

(32) Tsolou, G.; Mavrantzas, V. G.; Theodorou, D. N. *Macromolecules* **2005**, *38*, 1478.

(33) Valcarcel, J. P.; Palacios, J.; Alvarado-Gil, J. J. *J. Mater. Sci.* **1999**, *34*, 2113.

(34) Allen, M. P.; Tildesley, D. J. *Computer Simulation of Liquids*; Oxford University Press: New York, 1987.

(35) Brandrup, J.; Grulke, E. A.; Immergut, E. H. *Polymer Handbook*; Wiley-Interscience: New York, 1999.

(36) Buchenau, U.; Wischnewski, A. *Phys. Rev. B* **2004**, *70*, 092201.

(37) Huang, D. H.; Simon, S. L.; McKenna, G. B. *J. Chem. Phys.* **2005**, *122*, 084907.

(38) McQuarrie, D. A. *Statistical Mechanics*; Harper & Row: New York, 1976.

(39) English, N. J. *Mol. Phys.* **2008**, *106*, 1887.

(40) Nasrabad, A. E.; Oghaz, N. M.; Haghighi, B. *J. Chem. Phys.* **2008**, *129*, 024507.

(41) Sakiyama, Y.; Takagi, S.; Matsumoto, Y. *J. Chem. Phys.* **2005**, *122*, 234501.

(42) Keffer, D. J.; Edwards, B. J.; Adhangale, P. *J. Non-Newtonian Fluid Mech.* **2004**, *120*, 41.

(43) Saalwachter, K.; Burchard, W. *Macromolecules* **2001**, *34*, 5587.

(44) Das, S. K.; Horbach, J.; Binder, K.; Fisher, M. E.; Sengers, J. V. *J. Chem. Phys.* **2006**, *125*, 024506.

(45) Kroger, M.; Ilg, P. *J. Chem. Phys.* **2007**, *127*, 034903.

(46) Che, J. W.; Cagin, T.; Deng, W. Q.; Goddard, W. A. *J. Chem. Phys.* **2000**, *113*, 6888.

(47) Rosenbaum, E. J.; English, N. J.; Johnson, J. K.; Shaw, D. W.; Warzinski, R. P. *J. Phys. Chem. B* **2007**, *111*, 13194.

(48) Ungerer, P.; Nieto-Draghi, C.; Rousseau, B.; Ahunbay, G.; Lachet, V. *J. Mol. Liq.* **2007**, *134*, 71.

(49) Daivis, P. J.; Evans, D. J. *J. Chem. Phys.* **1995**, *103*, 4261.

(50) Dysthe, D. K.; Fuchs, A. H.; Rousseau, B. *J. Chem. Phys.* **2000**, *112*, 7581.

(51) Torii, D.; Nakano, T.; Ohara, T. *J. Chem. Phys.* **2008**, *128*, 282190.

(52) Lussetti, E.; Terao, T.; Muller-Plathe, F. *J. Phys. Chem. B* **2007**, *111*, 11516.

(53) Marechal, G.; Ryckaert, J. P. *Chem. Phys. Lett.* **1983**, *101*, 548.

(54) Bird, R. B.; Stewart, W. E.; Lightfoot, E. N. *Transport Phenomena*; John Wiley: New York, 2002.

(55) Bridgman, P. W. *Proc. Am. Acad. Arts Sci.* **1923**, *59*, 141.